

Multifunctional Additive Ethoxy(pentafluoro)cyclotriphosphazene Enables Safe Carbonate Electrolyte for SiO_x -Graphite/NMC811 Batteries

Sufu Liu,^[a] Maximilian Becker,^[a] Yuanye Huang-Joos,^[a] Huagui Lai,^[a] Gerrit Homann,^[a] Rabeb Grissa,^[a] Konstantin Egorov,^[a] Fan Fu,^[a] Corsin Battaglia,^[a, b] and Ruben-Simon Kühnel*^[a]

The silicon (Si) or silicon monoxide (SiO_x)-graphite (Gr)/nickel-rich $\text{LiNi}_x\text{Mn}_y\text{Co}_z\text{O}_2$ (NMC, $x+y+z=1$, with $x \geq 80\%$) cell chemistry is currently regarded as a promising candidate to further improve the energy density of rechargeable lithium-ion batteries, but is confronted with safety and cycling stability issues. Here, the flame retardant ethoxy(pentafluoro)cyclotriphosphazene (PFPN) is studied as electrolyte additive in the SiO_x -Gr/NMC811 full cell system. We find that PFPN in combination with an increased lithium hexafluorophosphate (LiPF_6) concentration renders carbonate-based electrolytes non-flammable based on a very low self-extinguishing time of 3.1 s g^{-1} while the electrolyte maintains a

high ionic conductivity of 8.4 mS cm^{-1} at 25°C . Importantly, PFPN in combination with fluoroethylene carbonate (FEC) also stabilizes the solid-electrolyte interphase of Si-based anodes beyond the level achieved only with FEC. Furthermore, PFPN improves the wetting property of the electrolyte, rendering it a multifunctional additive. As a result, excellent capacity retention of 87% after 200 cycles at 1 C was achieved for SiO_x -Gr/NMC811 pouch cells with a relatively high SiO_x content of 20%. Our work provides a promising avenue for developing safe and high-performance electrolytes for lithium-ion batteries with silicon-based anodes.

Introduction

In recent decades, portable electronic devices and electric vehicles have achieved great success owing to the successful commercialization of lithium-ion batteries (LIBs) while still being confronted with the challenge to further improve energy density.^[1,2] The silicon (Si) or silicon monoxide (SiO_x)-graphite (Gr)/nickel (Ni)-rich $\text{LiNi}_x\text{Mn}_y\text{Co}_z\text{O}_2$ (NMC, $x+y+z=1$, $x \geq 80\%$) cell chemistry is widely regarded as one of the most promising next-generation candidates to enhance the energy density of lithium-ion batteries and extend the driving range of electric vehicles beyond 500 km without making the vehicle excessively heavy.^[3,4] Si and SiO anodes can deliver capacities as high as 3579 mAh g^{-1} (theoretical for $\text{Li}_{15}\text{Si}_4$) and $\sim 1700 \text{ mAh g}^{-1}$ (practical), respectively, which is much higher than that of graphite (372 mAh g^{-1}). However, during continuous cycling, the huge

volume change of Si-based materials along with active material pulverization and repeated solid electrolyte interphase (SEI) formation leads to rapid capacity fading.^[5–8] Meanwhile, Ni-rich $\text{LiNi}_{0.8}\text{Mn}_{0.1}\text{Co}_{0.1}\text{O}_2$ (NMC811) cathodes can deliver a higher specific energy than LiFePO_4 , stoichiometric NMC111 or LiCoO_2 materials. However, NMC811 also comes with challenges such as performance degradation and safety issues related to the ease of oxygen release from the H_3 phase and its compatibility with organic carbonate-based electrolytes.^[9,10] In addition, the high flammability of carbonate solvents further reduces the intrinsic safety of LIBs based on Ni-rich NMC.^[11,12]

To solve the various challenges mentioned above, one of the most effective methods is to develop advanced electrolytes with flame-retardant property that also form stable electrode-electrolyte interphases. However, it is a great challenge to find an electrolyte formulation that can tackle the aggressive chemistry of Si-containing/Ni-rich LIBs. To date, various strategies have been proposed to render organic electrolytes non-flammable. Those include the use of anti-flame (co)solvents, highly concentrated electrolytes (HCE), localized high-concentration electrolytes (LHCE) and flame-retardant additives.^[13,14] However, the eco-friendliness of fluorinated compounds and compatibility of phosphate-type solvents during long-term cycling pose challenges when developing non-flammable (co)solvents that require a high content in the electrolyte.^[15,16] HCEs and LHCEs represent a relatively new approach to develop safe electrolytes for high-energy batteries, but both types of electrolytes are faced with high cost and low ionic conductivity (limiting fast-charging performance) and hence

[a] Dr. S. Liu, Dr. M. Becker, Dr. Y. Huang-Joos, H. Lai, Dr. G. Homann, Dr. R. Grissa, Dr. K. Egorov, Dr. F. Fu, Prof. Dr. C. Battaglia, Dr. R.-S. Kühnel
Empa – Swiss Federal Laboratories for Materials Science and Technology
8600 Dübendorf (Switzerland)

E-mail: ruben-simon.kuehnel@empa.ch

[b] Prof. Dr. C. Battaglia

ETH Zurich

Department of Information Technology and Electrical Engineering
8092 Zurich (Switzerland)

 Supporting information for this article is available on the WWW under
<https://doi.org/10.1002/batt.202300220>

 © 2023 The Authors. *Batteries & Supercaps* published by Wiley-VCH GmbH. This is an open access article under the terms of the Creative Commons Attribution License, which permits use, distribution and reproduction in any medium, provided the original work is properly cited.

are far from being industrially scalable.^[17–21] Meanwhile, in consideration of the balanced trade-offs between cost, scalability, improved safety and electrochemical compatibility, the use of flame-retardant additives is much more promising to develop next-generation non-flammable electrolytes.

Until now, many electrolytes based on well-known flame-retardant additives have been developed, such as triethyl phosphate (TEP),^[22] tris(2,2,2-trifluoroethyl) phosphate (TFP),^[23] poly[bis-(ethoxyethoxyethoxy)phosphazene] (EEEP),^[24] dimethyl methyl phosphate (DMMP),^[25,26] perfluoro-2-methyl-3-pentanone (PFMP),^[27] etc. However, all these phosphorus-containing additives have been reported to diminish the electrochemical compatibility of the electrolyte with graphite anodes due to solvent co-intercalation, resulting in graphite exfoliation.^[13] Recently, one of the fluorinated cyclic phosphazenes, ethoxy(pentafluoro)cyclotriphosphazene (PFPN), has shown great promise as flame-retardant-type additive that does not seem to impair electrochemical performance. Xia et al. found that 5 wt.% PFPN can effectively suppress the flammability of 1 M lithium hexafluorophosphate (LiPF₆) in ethylene carbonate (EC):dimethyl carbonate (DMC) (3:7 by vol.) electrolyte and demonstrated excellent compatibility with both graphite anode and LiCoO₂ cathode.^[28] It was also shown to improve the high-voltage cycling performance of LiCoO₂ half cells up to 4.5 V. Furthermore, Dagger et al. found that PFPN not only displays excellent flame retardancy but also has no impact on the cycling performance of 4.2 V graphite/NMC111 cells.^[29] Moreover, Liu et al. found that PFPN helps to form a dense, uniform and thin protective layer on the surface of LiNi_{0.5}Mn_{1.5}O₄ cathode materials, protecting the structure from disruption up to 4.9 V.^[30] Hence, it has been demonstrated that the PFPN additive has outstanding flame-retardant properties and can improve the electrochemical performance of graphite-based LIBs, especially at high voltage. However, there is no study about the compatibility of PFPN with Si (or SiO_x) anodes and Ni-rich NMC cathodes yet, which is an interesting and worthwhile study as part of the development of next-generation LIBs (an overview about the existing studies with PFPN can be found in Table S1).

In this work, we developed a new formulation of a safe carbonate electrolyte for SiO_x-Gr/NMC811 LIBs. Based on commercially available carbonate solvents, our designed electrolyte, 1.35 M LiPF₆ in EC/ethyl methyl carbonate (EMC) (3:7 by vol.) with 10 wt.% fluoroethylene carbonate (FEC) and 5 wt.% PFPN, displays a self-extinguishing time (SET) of only 3.1 s g⁻¹ due to the presence of PFPN and the increased LiPF₆ concentration. Meanwhile, this non-flammable electrolyte maintains a high ionic conductivity of 8.4 mS cm⁻¹ at 25 °C and also displays improved separator wettability due to the outstanding wetting properties of PFPN. When coupled with SiO_x-Gr/NMC811 electrodes, an enhanced electrochemical performance is found for our electrolyte, both in coin and pouch cells. For the first time, it is disclosed that PFPN contributes more to the SEI stability of SiO_x-based anodes due to its preferential reduction, forming a LiF-rich interphase, which helps to suppress the pulverization of the anode due to the volume change of Si.

Results and Discussion

Physicochemical properties of various electrolytes

Starting from a baseline electrolyte (BE) consisting of 1 M LiPF₆ in EC:EMC (3:7 by vol.), the self-extinguishing time (SET) of various electrolytes with different LiPF₆ concentrations and additives (FEC and/or PFPN) can be found in Figure S1. Following the suggestion by Xu et al., we consider an electrolyte with an SET value of less than 6 s g⁻¹ as non-flammable.^[23,31] The baseline electrolyte and the baseline electrolyte plus 10 wt.% FEC (denoted as BE 10% FEC) display SETs of 65 s g⁻¹ and 67 s g⁻¹, respectively, revealing that FEC does not suppress the flammability of the electrolyte although it is a fluorinated compound. With increasing LiPF₆ concentration and upon addition of the flame-retardant additive PFPN, the SET decreases as revealed by the results of 57.5 s g⁻¹ for 1.35 M BE (1.35 M LiPF₆ in EC-EMC (3:7 by vol.)) and 9.9 s g⁻¹ for BE with 5 wt.% PFPN. Interestingly, when combining PFPN with an increased LiPF₆ concentration and FEC in an electrolyte with a composition of 1.35 M LiPF₆ in EC:EMC (3:7 by vol.) with 5 wt.% PFPN and 10 wt.% FEC (denoted as modified electrolyte (ME)) an outstanding flame retardancy as reflected by an SET value of only 3.1 s g⁻¹ is obtained. Therefore, the LiPF₆ concentration was increased from the common value of 1.0 M to 1.35 M to obtain a non-flammable electrolyte with a flame-retardant content of only 5 wt%. As shown in Figure 1(a), for the electrolytes with 5 wt.% PFPN, the SET decreases from 9.9 to 0 s g⁻¹ when increasing the LiPF₆ concentration from 1.0 to 1.35 M. Also, for the electrolytes with 10% FEC and 5 wt.% PFPN, the SET decreases from 12.4 to 3.1 s g⁻¹ when increasing the LiPF₆ concentration from 1.0 to 1.35 M. In contrast, only increasing the LiPF₆ concentration to 1.35 M without addition of the flame retardant has a relatively much smaller effect on the SET of the electrolyte (Figure S1). Hence, a synergistic effect for non-flammability has been achieved by increasing the LiPF₆ concentration beyond the standard concentration of 1.0 M in the presence of 5 wt.% of the flame retardant PFPN for all the electrolytes with or without FEC. Meanwhile, for the electrolyte with only 1 M LiPF₆, a significantly higher amount of flame retardant, ca. 10 wt.%, would be required to achieve excellent flame retardancy, which would come at a significantly higher cost and conductivity penalty. Ultimately, the choice of LiPF₆ concentration (and flame-retardant content) depends on the chosen trade-off between flammability, ionic conductivity and electrolyte cost. Based on our experimental data, the composition selected by us represents a good comprise between these properties. The ionic conductivity of some other electrolytes is also measured in Figure S2. BE and BE 10% FEC display very similar values of ca. 9.3 mS cm⁻¹ at 25 °C. With increasing amount of PFPN additive or LiPF₆ salt concentration, the ionic conductivity gradually decreases. However, the non-flammable electrolyte ME still maintains a high value of 8.4 mS cm⁻¹, around 90% of the conductivity of BE 10% FEC.

The viscosity of different electrolytes between 0 and 40 °C is displayed in Figure S3. At 25 °C, ME displays a slightly higher viscosity (4.8 mPas) than BE 10% FEC (3.5 mPas), which can be

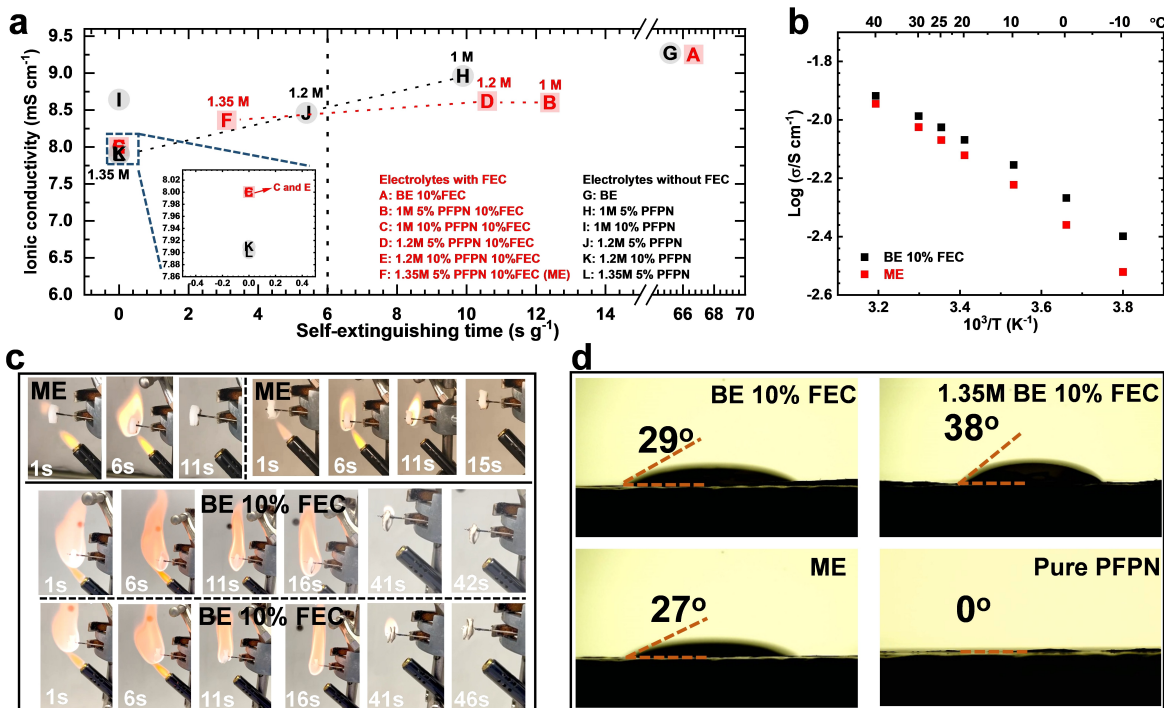


Figure 1. a) Ionic conductivity and self-extinguishing time of some typical electrolytes considered for this study; b) Arrhenius plots of the ionic conductivity of BE 10% FEC and ME; c) representative snapshots illustrating the combustion process of BE 10% FEC and ME during the SET experiment; d) contact angle between Celgard 2500 separator foil and various electrolytes and pure PFPN. The baseline electrolyte (BE) was 1.0 mol/L LiPF₆ in EC/EMC (3:7, by vol.). "1.35 M" denotes an increased LiPF₆ concentration of 1.35 mol/L.

ascribed to the higher salt concentration of ME. The temperature dependence of the conductivity of BE 10% FEC and ME is illustrated as Arrhenius plots in Figure 1(b). With increasing temperature, the difference in conductivity between the two electrolytes narrows, as can be expected from the higher LiPF₆ concentration of ME. The difference in combustion of BE 10% FEC and ME during the SET experiment is illustrated in Figure 1(c) by photographs taken at different time after ignition for two independent samples each: it can be clearly seen that ME rapidly ceases burning after the flame is stopped while BE 10% FEC burns for a long time.

To demonstrate the beneficial effect of PFPN on the wetting properties of carbonate electrolytes, the contact angle between different electrolytes and Celgard 2500 separator foil was measured as shown in Figure 1(d). The electrolyte 1.35 M BE with 10% FEC exhibits a much larger contact angle (38°) compared to BE 10% FEC (29°), indicating that a higher LiPF₆ concentration decreases the wettability of the electrolyte. Interestingly, despite having also an increased LiPF₆ concentration, our designed electrolyte ME displays a smaller contact angle (27°) than BE 10% FEC. This finding indicates that PFPN significantly improves the wetting between carbonate electrolytes and polyolefin separators. This assertion is confirmed by the instantaneous wetting of Celgard 2500 by pure PFPN as illustrated by the photographs shown in Figure S4 and Supplementary Video 1. This enhanced wettability of carbonate electrolytes with PFPN suggests that PFPN also helps to homogenize Li⁺ concentration gradients on the surface of active material particles, thus rendering lithium intercalation/

deintercalation more uniform, especially at high cycling rates.^[32,33]

Coin cell cycling experiments

The electrochemical performance of BE 10% FEC and our designed electrolyte ME was firstly evaluated in half and full coin cells. After two formation cycles at C/20, the SiO_x-Gr anode with a SiO_x content of 20% displayed an areal capacity of around 2.9 mAh cm⁻² at 0.2 C/0.5 C (charge/discharge) in both BE 10% FEC and ME (Figure 2a). Remarkably, after 150 cycles our designed electrolyte significantly outperforms BE 10% FEC with a capacity retention of 48.5% compared to 41.6%. The cycling result of Li/NMC811 half cells is provided in Figure 2(b). After 270 cycles, the cells with the BE 10% FEC and ME electrolytes maintain 84.6% and 87.3% of their initial capacity after formation, respectively. From the results above, it can be expected that capacity degradation of SiO_x-Gr/NMC811 full cells mainly stems from the anode and that our designed electrolyte improves the cycling stability of both the anode and the cathode, with a major improvement for the anode.

The rate and long-term cycling performance of full cells was also investigated for BE 10% FEC and ME. As shown in Figure 2(c), full cells with both electrolytes display similar performance at rates of ≤ 0.5 C during a rate test. However, we find a higher capacity with ME for rates of ≥ 1 C, especially at the highest applied rate of 3 C. The cells with ME offer an average capacity of 2.19 mAh cm⁻² at 2 C and 1.48 mAh cm⁻² at

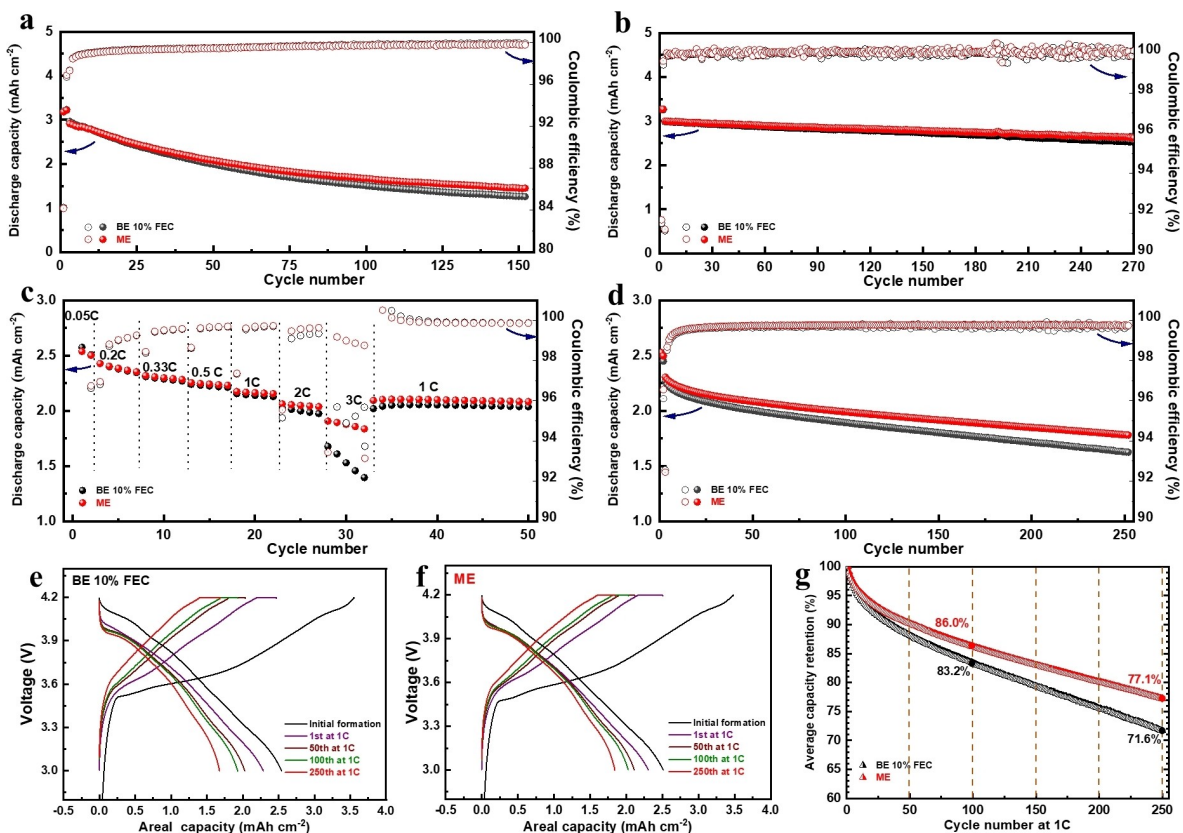


Figure 2. a, b) Discharge capacity and Coulombic efficiency of a) Li/SiO_x-Gr and b) Li/NMC811 half cells cycled at 0.2 C/0.5 C (charge/discharge); c) rate performance and d) long-term cycling performance at 1 C of SiO_x-Gr/NMC811 full cells; e, f) charge/discharge profiles of selected cycles of the cells shown in (d) with e) BE 10% FEC or f) ME as electrolyte and g) capacity retention of the cells shown in (d).

3 C during the 5 cycles at each of these rates (1 C = 2.80 mAh cm⁻²). In contrast, full cells with BE 10% FEC display a much lower rate capability (2.09 mAh cm⁻² at 2 C and 1.07 mAh cm⁻² at 3 C), suggesting inferior Li intercalation/deintercalation kinetics at high rates. We ascribe the improved rate performance of the full cells despite the lower conductivity of the modified electrolyte to the improved wetting properties of the electrolyte due to the presence of PFPN as discussed above (see again Figure 1d) and the lower electrode resistance as discussed below (Figure S18). The long-term stability of SiO_x-Gr/NMC811 full cells cycled at 1 C between 3.0–4.2 V is presented in Figures 2(d–g). Inspection of Figure 2(d) shows that both electrolytes result in a similar initial capacity of around 2.30 mAh cm⁻² after formation, but then the cells start to diverge slightly in subsequent cycles with higher capacity retention for ME. As displayed in Figure 2(g), the cell with ME presents a capacity retention of 86.0% after 100 cycles compared to 83.2% for BE 10% FEC. This improvement in cycling stability is even more pronounced after 250 cycles, with 77.1% for ME and 71.6% for BE 10% FEC. The typical voltage-capacity profiles along various cycles using BE 10% FEC (Figure 2e) and ME (Figure 2f) are also compared for voltage hysteresis and stability. It can be clearly seen that the cell with ME keeps the charge and discharge cell voltage better than the one with BE 10% FEC. In summary, although showing a comparatively lower ionic conductivity than BE 10% FEC, our

designed safe electrolyte ME actually improves both the cycling stability as well as the rate performance of SiO_x-Gr/NMC811 full cells. We ascribe the improved cycling stability with the modified electrolyte to better stabilization of the electrode-electrolyte interfaces due to the enhanced SEI and CEI stability as discussed below (Figures 3 and 4).

Evolution of electrode morphology during cycling

The morphology change of both the SiO_x-Gr anode and the NMC811 cathode after cycling for 250 cycles at 1 C (electrochemical results shown in Figure 2d) was characterized using scanning electron microscopy (SEM). All electrodes for this investigation were soaked and rinsed in pure EMC to remove electrolyte salt residues and subsequently dried. The typical morphology of the SiO_x-Gr anode before cycling is presented in Figure S5. The thickness of the active material layer was around 48.5 µm. It can be seen that the SiO_x particles are well dispersed between the graphite particles. The graphite particles appear darker in the backscattered electrons (BSE) mode while the SiO_x particles appear brighter in color as they consist of heavier elements than the carbon of graphite (Figure S5b). Meanwhile, the micrometer-sized graphite particles display the typical layered sheet structure and the SiO_x particles have an irregular block-shape morphology with a size of several micrometers.

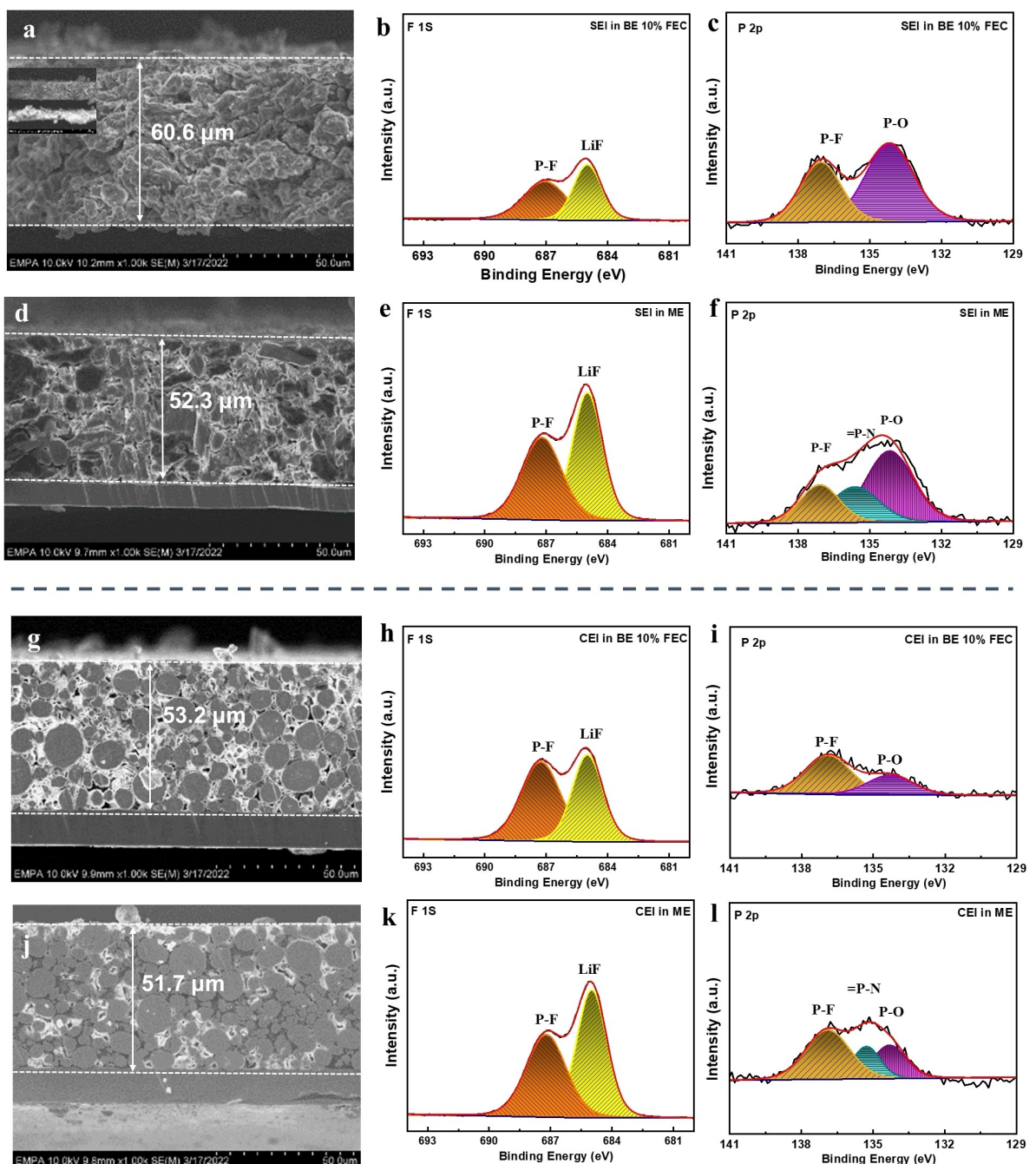


Figure 3. Cross-sectional SEM images and typical F 1s and P 2p XPS spectra of the $\text{SiO}_x\text{-Gr}$ anode after cycling in a–c) BE 10% FEC and d–f) ME electrolytes; cross-sectional SEM images and typical F 1s and P 2p XPS spectra of the NMC811 cathode after cycling in g–i) BE 10% FEC and j–l) ME electrolytes. The $\text{SiO}_x\text{-Gr}$ anodes and NMC811 cathodes were extracted from the full cells shown in Figure 2(d).

After 250 cycles at 1 C, a morphological and compositional investigation of the surface of the $\text{SiO}_x\text{-Gr}$ anodes was carried out via SEM and EDS, respectively, as shown in Figures S6 and S7. We find that both SiO_x and graphite particles are covered on the surface with a layer that appears blurred and rough, which is mainly the result of the high sensitivity of the focused electron beam to these electrolyte decomposition products with low electronic conductivity. From the top view, it can be seen that the gap between gray and black particles is slightly larger for BE 10% FEC (Figure S6b) than for ME (Figure S7b).

However, the EDS maps of the probed elements are quite similar. Larger differences are visible in cross-sectional SEM images as shown in Figure 3(a and d). After 250 cycles at 1 C, the $\text{SiO}_x\text{-Gr}$ anode extracted from the BE 10% FEC cell presents a thickness of around 60.6 μm , while the thickness is only around 52.3 μm for ME. The morphology evolution of the NMC811 cathode was also characterized. Figure S8 shows SEM images of the pristine electrode. The polycrystalline NMC811 particles have a diameter range of around 5–10 μm . After long-term cycling, cracks appeared inside the NMC811 electrode for

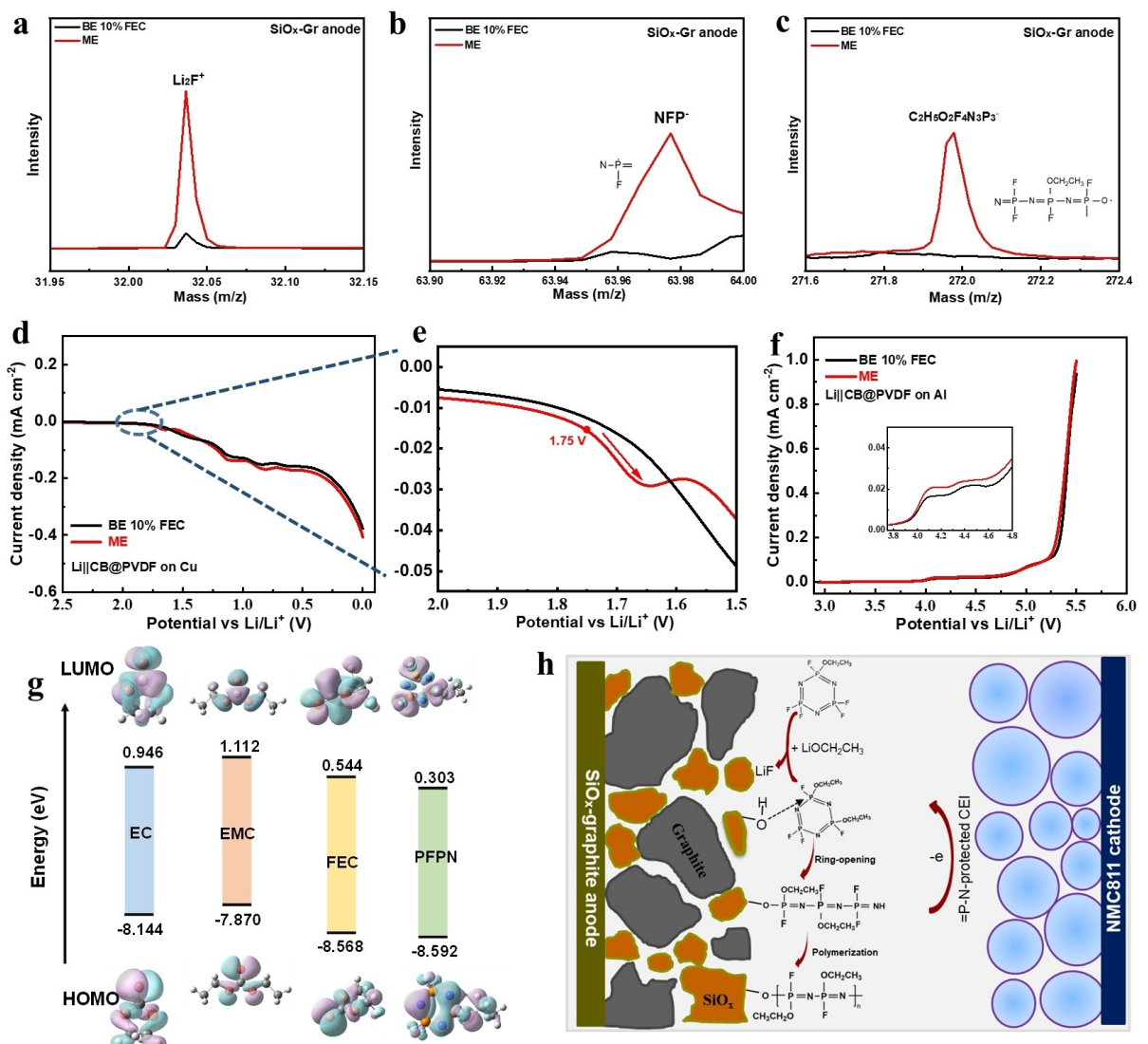


Figure 4. a–c) ToF-SIMS spectra of the $\text{SiO}_x\text{-Gr}$ anode after cycling in BE 10% FEC or ME for selected m/z ranges; d–f) linear sweep voltammograms of BE 10% FEC and ME (scan rate: 1 mV s⁻¹, 25 °C, working electrode: d, e) PVDF@CB coated on Cu for the cathodic scan, f) PVDF@CB coated on Al for the anodic scan; g) frontier molecular orbital levels of carbonate solvents (EC, EMC, FEC) and PFPN; h) schematic illustration of the decomposition routes of PFPN on $\text{SiO}_x\text{-Gr}$ anode surface. The $\text{SiO}_x\text{-Gr}$ anodes for the ToF-SIMS experiment were extracted from the full cells shown in Figure 2(d).

both electrolytes as visible both in the top view and cross-sectional SEM images (Figures S9 and S10), in line with the observed voltage polarization and capacity fading. Meanwhile, the cathode thickness after cycling is slightly smaller for ME (51.7 μm , Figure 3j) than for BE 10% FEC (53.2 μm , Figure 3g). These results demonstrate that our designed electrolyte effectively suppresses the expansion of the $\text{SiO}_x\text{-Gr}$ anode and the NMC811 cathode during charge-discharge cycling.

Interphase stabilization by PFPN

X-ray photoelectron spectroscopy (XPS) was employed to unveil the SEI and CEI forming on the $\text{SiO}_x\text{-Gr}$ anode and NMC811 cathode, respectively, during cycling in the electrolytes BE 10% FEC and ME (Figure 3). As for the XPS measure-

ments and the time-of-flight secondary ion mass spectrometry (ToF-SIMS) measurements discussed in the next paragraph, electrodes that were subjected to 250 cycles at 1 C in full coin cells (Figure 2d) were investigated. For both electrolytes, the SEI consists of organic compounds (C–O and C–C peaks) and inorganic compounds such as Li_xPF_y , LiF and Li_2CO_3 , revealing the typical mixed organic-inorganic nature of the SEI forming in carbonate electrolytes.^[34] However, the F 1s spectra show a much stronger LiF signal (at 685.0 eV) upon incorporation of PFPN (ME), indicating defluorination of PFPN on the surface of the $\text{SiO}_x\text{-Gr}$ anode (Figures 3b and e). Analysis of the P 2p spectra shown in Figure 3(c and f) indicates that PFPN also decomposes into =P–N-containing compounds in the SEI. Meanwhile, the presence of PFPN results in no significant compositional differences for the O 1s and C 1s spectra (Figure S11). However, we find a reduction of the C=O peak

area for ME compared to BE 10% FEC, indicating that the decomposition of carbonate solvents is suppressed in our designed electrolyte. The near-surface post-mortem elemental composition of the SEI as seen by XPS is summarized in Figure S12 for both electrolytes. We find a higher fraction of Li, F, Si and P and a lower fraction of C and O at the surface of the anode for ME compared to BE 10% FEC. This demonstrates that the SEI formed in the presence of PFPN is relatively richer in inorganic components, especially LiF. For the NMC811 cathode, the P 2p spectra (Figures 3i, l) indicate the presence of additional species for the PFPN-containing electrolyte ME, indicating decomposition of PFPN also on the NMC811 cathode. In particular, the peak at 135.5 eV can be attributed to =P—N moieties.^[30,35]

In addition, ToF-SIMS measurements were performed to study the SEI in more detail. The mass spectra of selected compounds ablated post-mortem from the surface of the anode are shown in Figures 4(a–c), which also depict the corresponding chemical structures. We find a much stronger Li_2F^+ signal for ME on the surface of the anode recovered after 250 cycles at 1 C compared to BE 10% FEC, consistent with the XPS results. Furthermore, we find phosphazene derivatives/fragments such as NFP^- and $\text{C}_2\text{H}_5\text{O}_2\text{F}_4\text{N}_3\text{P}_3^-$ on the surface of the cycled anode, indicating that the SEI contains additional decomposition products of PFPN besides LiF. To exclude that these signals stem from interactions of the ion beam with PFPN, we repeated the SIMS experiment with anodes extracted from cells that were not subjected to charge/discharge cycling. As shown in Figure S15, we find no clear signals for the m/z values corresponding to NFP^- and $\text{C}_2\text{H}_5\text{O}_2\text{F}_4\text{N}_3\text{P}_3^-$ on the anode surface when simply resting the cells for 24 hours. Hence, there is strong indication that these P—N moieties stem indeed from electrochemical decomposition of PFPN or from the reaction of other electrochemically formed compounds with PFPN. Moreover, we find that certain PFPN derivatives such as $\text{C}_4\text{H}_{10}\text{O}_2\text{F}_4\text{N}_3\text{P}_3^-$ are only present before washing the electrode with EMC (Figure S16), indicating that certain PFPN reaction products are soluble in the carbonate electrolyte.^[36] We emphasize that such soluble chemicals are only intermediate components, which could further join the interphase formation and does not reveal SEI instability as further shown by leakage current measurement: As shown in Figure S17, we applied an additional 3 hour hold at 4.2 V after two formation cycles at C/20 and a constant current-constant voltage (CCCV) charge at 1 C. BE 10% FEC and ME result in a leakage current density of $10.3 \mu\text{A cm}^{-2}$ and $9.1 \mu\text{A cm}^{-2}$ after 60 minutes, respectively, which decay exponentially to $3.3 \mu\text{A cm}^{-2}$ and $3.1 \mu\text{A cm}^{-2}$, respectively, after the full 180 minutes period. The reduced oxidation current in our designed electrolyte further confirms the improved interphase stability. Besides, considering that the electrolyte developed in this study significantly enhances the cycling stability of both coin and pouch cells vs. the FEC-based baseline electrolyte, we conclude that the SEI stability is not limited by potential solubility of PFPN reaction products but rather benefits from the presence of PFPN.

The electrochemical stability of BE 10% FEC and ME was also evaluated by linear sweep voltammetry (LSV) using three-

electrode cells with carbon black-based working electrodes. As shown in Figure 4(d and e), the voltammogram for the electrolyte with PFPN (ME) shows a distinct feature between 1.75 and 1.65 V vs. Li/Li^+ during the cathodic scan that is absent for BE 10% FEC, indicating that PFPN is reduced on the $\text{SiO}_x\text{-Gr}$ surface prior to the other components of the electrolyte (carbonate solvents and LiPF_6 salt). Meanwhile, as shown in Figure 4(f), both electrolytes demonstrate similar oxidative stability of ca. 4.6 V vs. Li/Li^+ (based on a current density of $25 \mu\text{A cm}^{-2}$). This finding differs from previous reports that PFPN is likely oxidized on the cathode prior to the decomposition of other components of carbonate electrolytes.^[30] This difference might be related to differences in solvation structure between our electrolyte and other electrolytes reported in literature as well as differences in the catalytic activity of the employed working electrodes. The energy of the molecular orbitals of PFPN and the carbonate solvents (EC, EMC, FEC) was also analyzed. According to the frontier molecular orbital theory, a lower energy of the highest occupied molecular orbital (HOMO) renders a molecule more stable against oxidation, while a lower energy of the lowest unoccupied molecular orbital (LUMO) makes the molecule easier to be reduced. As shown in Figure 4(g), the LUMO energy of PFPN is lower than that of the carbonate solvents (EC, EMC and FEC). Meanwhile, the HOMO energy of PFPN is notably lower compared to these carbonates due to the strong electron-withdrawing effect of the fluorine atoms of PFPN. Based on this calculation, and ignoring the actual reaction products and interactions with other electrolyte components or active materials, PFPN is more prone to reduction on the anode and more stable against oxidation on the cathode than EC, EMC and FEC.

Moreover, during a CV measurement of the $\text{SiO}_x\text{-Gr}/\text{NMC811}$ full cell (Figure S18), a small oxidation current did appear at 3.5 V in the first cycle of the cell with PFPN, which can be attributed to the electrochemical decomposition of PFPN. In addition, the first phase transition peak from hexagonal (H1) to monoclinic (M) for NMC811 is reduced by around 65 mV, indicating decreased polarization of the $\text{SiO}_x\text{-Gr}/\text{NMC811}$ full cell due to the formation of a less resistive CEI. The cell impedance during cycling was also measured using electrochemical impedance spectroscopy (EIS, Figure S19). The EIS spectra usually consist of the Ohmic resistance of the cell, R_o , the interfacial resistance of Li^+ migrating through the interphase films, R_i , the charge-transfer resistance, R_{ct} , and the Warburg impedance, R_w , describing the diffusion of Li^+ inside the active material particles. The two semicircles at high frequencies in a Nyquist plot can be attributed to R_i and R_{ct} .^[37] This analysis results in smaller resistances for our designed electrolyte, revealing improved kinetics with PFPN.

Based on our XPS, ToF-SIMS, and electrochemical characterizations discussed above, we propose the following mechanism for the interphase stabilization of the $\text{SiO}_x\text{-Gr}$ anode in the presence of PFPN (Figure 4h): Specifically, our results indicate that a substitution reaction takes place between PFPN and lithium alkoxides such as lithium ethoxide, which are well-known reduction products of EMC,^[38] resulting in LiF and

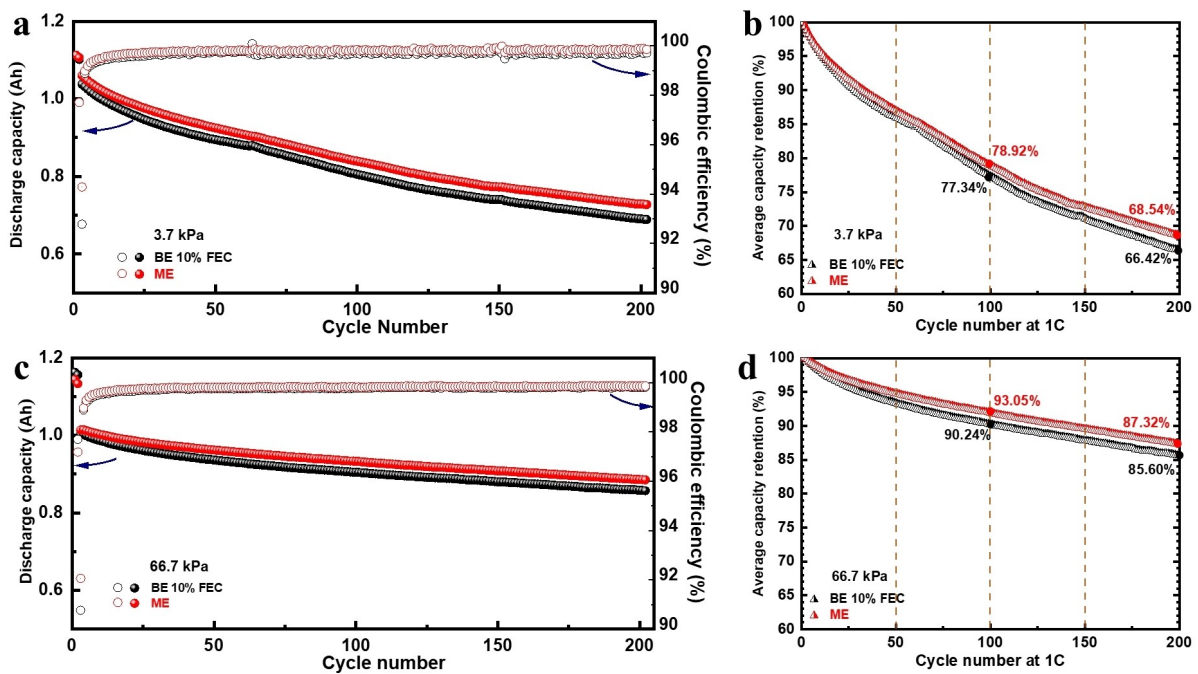


Figure 5. a, c) Discharge capacity and Coulombic efficiency as well as b, d) capacity retention of 1 Ah $\text{SiO}_x\text{-Gr}/\text{NMC}811$ pouch cells with BE 10% FEC or ME as electrolyte. The cells were cycled at 1 C under different pressures of a, b) 3.7 kPa and c, d) 66.7 kPa.

fluorine-poorer PFPN derivatives with additional alkoxy groups (such as $\text{C}_4\text{H}_{10}\text{O}_2\text{F}_4\text{N}_3\text{P}_3$ in Figure S16). Meanwhile, we find good indication that this reaction is followed by ring-opening and polymerization reactions, as indicated by the $=\text{P}-\text{N}$ -containing compounds we found in the SEI (measured by XPS, see again Figure 3), as well as the NFP^- , $\text{C}_2\text{H}_5\text{O}_2\text{F}_4\text{N}_3\text{P}_3^-$ signals (measured by ToF-SIMS, see again Figure 4). It is possible that the PFPN derivatives undergo nucleophilic attack by the electron-rich oxygen atoms of hydroxyl groups known to be present on the surface of SiO_x particles,^[39–41] inducing the ring-opening reaction and subsequent polymerization. We emphasize that these proposed reactions are based on our experiment results. However, a deeper mechanistic study utilizing other advanced computational methods as well as experimental characterization techniques such as ion chromatography and liquid chromatography-mass spectrometry is still needed to fully understand the SEI formation in the presence of PFPN. It was also previously reported that such polyphosphazene-type compounds contribute to the stability of the CEI,^[35,42,43] which is also validated by the XPS results shown in Figure 3. In summary, our work shows that the presence of PFPN in the electrolyte results in the formation of more effective protective layers on $\text{SiO}_x\text{-Gr}$ and NMC811 that are richer in LiF and that contain $=\text{P}-\text{N}$ -based compounds, likely polyphosphazenes. The changes in layer composition are more pronounced for the SEI, which is consistent with the half-cell cycling data where a larger improvement in capacity retention with PFPN was found for the $\text{SiO}_x\text{-Gr}$ anode.

Pouch cell cycling performance

Moreover, the impact of PFPN was also investigated in 1 Ah $\text{SiO}_x\text{-Gr}/\text{NMC}811$ pouch cells. As shown in Figure S20, the pouch cells were fastened inside rigid holders made of plastic and aluminum. The setup also contained a pressure sensor and the initial pressure was set to 3.7 or 66.7 kPa. The long-term cycling performance of these pouch cells using BE 10% FEC or ME as electrolyte is displayed in Figure 5. The cells were cycled at 1 C between 3.0 and 4.2 V. Under a pressure of 3.7 kPa, the cell with BE 10% FEC delivered a capacity retention of 77.3% after 100 cycles at 1 C, while the cell with ME reached a capacity retention of 78.9% under the same conditions. After 200 cycles, the capacity dropped to 66.4% and 68.5% of the initial value for BE 10% FEC and ME, respectively. When applying an initial pressure of 66.7 kPa, the cell delivered a further improved capacity retention of 93.1% after 100 cycles for ME, 2.8% higher than for BE 10% FEC. After 200 cycles, a relative capacity of 87.3% and 85.6% was maintained for ME and BE 10% FEC, respectively. The higher pressure of 66.7 kPa clearly improves the cycling stability of these Si-based full cells, of which the main effect was attributed to the volume expansion restriction of the SiO_x particles under pressure.^[8] The pouch cell results confirm that the presence of PFPN in the electrolyte improves the cycling stability of $\text{SiO}_x\text{-Gr}/\text{NMC}811$ full cells.

Conclusions

In this work, ethoxy(pentafluoro)cyclotriphosphazene (PFPN) is proposed as a multifunctional electrolyte additive for the SiO_x -

Gr/NMC811 full cell system. Specifically, outstanding flame retardancy with a self-extinguishing time of 3.1 s g^{-1} has been achieved when adding 5 wt.% PFPN to an EC-EMC-FEC-LiPF₆ baseline electrolyte and simultaneously increasing the LiPF₆ concentration from 1.0 to 1.35 M while the electrolyte maintains a high ionic conductivity of 8.4 mS cm^{-1} at 25°C . Meanwhile, the presence of PFPN renders the SEI of the SiO_x-Gr anodes rich in LiF and effectively suppresses the volume expansion of the electrode. Combined with a more stable CEI derived from PFPN, our designed electrolyte helps to harness the aggressive chemistries of both Si-based anodes and Ni-rich NMC cathodes with robust interphases. Furthermore, PFPN also improves the wetting of polyolefin separators by carbonate electrolytes. As a result, our modified electrolyte enables significantly improved cycling stability of SiO_x-Gr/NMC811 full cells compared to the FEC-based baseline electrolyte as shown for coin cells and 1 Ah pouch cells. In summary, PFPN is a promising electrolyte additive for lithium-ion batteries with silicon-based anodes as it delivers significant improvements in terms of electrochemical performance, safety and wetting properties.

Experimental Section

Materials: 1 M LiPF₆ in EC-EMC (3:7 by vol.) was provided by Solvionic. LiPF₆ and FEC were purchased from Gotion and E-Lyte Innovations GmbH, respectively, all in battery grade. Ethoxy(pentafluoro)cyclotriphosphazene (PFPN, >98%) was purchased from Tokyo Chemical Industry (TCI). Prior to use, PFPN and FEC were dried over 3 Å molecular sieve. Electrolytes with different LiPF₆ concentrations and additive contents were prepared by adding various amount of salt and additives to the 1 M LiPF₆ in EC-EMC (3:7 by vol.) electrolyte. The complete compositions and designations for the electrolytes used in this study are provided in Table S2. Dry 1 Ah SiO_x-Gr/NMC811 pouch cells with a SiO_x content of the anode of 20% were purchased from Li-Fun Technology. The electrodes for the coin cell experiments were extracted from pouch cells and were punched into discs with a diameter of 12 mm (SiO_x-Gr anode) or 11 mm (NMC811 cathode) and dried at 120°C under vacuum for 12 h before use. The Li metal foil was purchased from China Energy Lithium.

Characterizations: A BioLogic MCS-10 multi-channel conductivity meter was used to measure the ionic conductivity of the electrolytes within a temperature range of -10 to 40°C . A Kyoto Electronics EMS-1000 spinning sphere viscometer was used for the determination of electrolyte viscosity with the motor speed set to 1000 rpm. All conductivity and viscosity measurements were repeated once and the average values are reported. Flammability was measured in a home-made setup as published in our previous work.^[44] The burning time of the electrolytes was measured ten times using 400 µL electrolyte and four layers of Whatman glass-fiber separators (GF/D, 12 mm diameter). The electrolytes were ignited by a 750°C stormproof lighter for 10 s and the SET was calculated as the burning time after ignition divided by the electrolyte mass. A digital camera (dnt DigiMicro Scale) was used to take photographs of selected electrolytes during the wetting of separators. Contact angles were measured after five seconds of vertically dropping 35 µL of electrolyte onto the surface of Celgard 2500 separator foil. The electrode morphology was characterized by SEM (FEI NanoSEM 230). The cross-sectional samples were prepared with an argon ion mill (Hitachi IM4000Plus) and cooled to

-70°C prior to milling to avoid the melting of organic binder. Energy-dispersive X-ray spectroscopy (EDS) maps were recorded with a tabletop SEM (Hitachi TM3030Plus). XPS was conducted with a PHI Quantum 2000 photoelectron spectrometer with a monochromated Al K_α X-ray source (1486.6 eV) with a pass energy of 30 eV. The binding energy values were referenced to the C1s peak (284.6 eV). A ToF-SIMS system (ION-TOF) was used to obtain mass spectrometry data, which used a primary 25 keV Bi³⁺ beam with a total current of 0.38 pA. If not otherwise specified, all electrodes were rinsed in EMC several times to remove residual electrolyte and dried under Ar before characterization.

Electrochemical measurements: Anodes and cathodes had an areal capacity of 3.5 and 2.8 mAh cm^{-2} , respectively, resulting in an N/P ratio of 1.25. The electrochemical performance of the coin cells was examined using 2032 type coin cells with two spacers (1 mm and 0.5 mm), a 1.4 mm spring, and a 16 mm Celgard 2500 separator and were assembled in an Ar-filled glove box. The electrolyte volume was set to 35 µL for full cells and 80 µL for half cells. For the formation of the full cells, the cells were first charged to 1.5 V at C/3 to minimize corrosion of the Cu current collector before a rest period of 12 h, followed by two formation cycles at C/20. Then, long-term cycling was carried out between 3.0–4.2 V with a constant voltage step at 4.2 V until the current dropped below C/20. Li/NMC811 and Li/SiO_x-Gr half cells were cycled in a voltage range of 2.8–4.3 V and 5 mV–1.5 V, respectively. A protocol of C/5 for charging (as defined as lithium deposition on the lithium metal counter electrode) and C/2 for discharging (as defined as lithium stripping from the lithium metal counter electrode) was applied to alleviate dendrite growth in half cells.^[45] The 1 Ah pouch cells were filled with ca. 3.8 mL of electrolyte and sealed prior to the cycling experiments. After formation, the pouch cells were degassed and resealed. Charge/discharge cycling data were recorded on BCS-805 (BioLogic) or CT3001A (Wuhan LAND Electronic) battery cyclers. In addition, linear sweep voltammetry (LSV), cyclic voltammetry (CV), and electrochemical impedance spectroscopy (EIS) were conducted on a BioLogic VMP3 potentiostat. All electrochemical measurements were conducted at 25°C .

Computational details: All density functional theory (DFT) calculations were performed with the Gaussian 16 software package. The molecular geometries for the ground states were optimized via DFT at the B3LYP/6-311G (d, p) level. The energy and electrostatic potential surfaces of molecules were evaluated at the B3LYP/6-311G (d, p) level as well. The overall bulk solvent effect was estimated using the solvation model based on density (SMD).^[46] During the calculations, acetone was used to represent the solvents due to the relatively close dielectric constants.

Acknowledgments

The authors thank the European Union for funding this work through the project "SeNSE". This project has received funding from the European Union's Horizon 2020 research and innovation program under grant agreement No. 875548. The authors would like to acknowledge the work of the University of Münster, Germany, their collaboration partner in the SeNSE project, who independently conducted similar experiments and came to similar conclusions.^[47] The authors thank Solvionic for providing the carbonate electrolyte and Marcel Held from Empa for providing expertise and equipment for the pouch cell experiments. Open Access funding provided by ETH-Bereich Forschungsanstalten.

Conflict of Interests

The authors declare no conflict of interest.

Data Availability Statement

The data that support the findings of this study are available from the corresponding author upon reasonable request.

Keywords: interphase modification · multifunctional additive · non-flammable electrolyte · pouch cells · Si-based anode

- [1] J. B. Goodenough, K. S. Park, *J. Am. Chem. Soc.* **2013**, *135*, 1167–1176.
[2] K. Xu, *Chem. Rev.* **2014**, *114*, 11503–11618.
[3] S. S. Zhang, *Energy Storage Mater.* **2020**, *24*, 247–254.
[4] J. Amici, P. Asinari, E. Ayerbe, P. Barbour, P. Bayle-Guillemaud, R. J. Behm, M. Berecibar, E. Berg, A. Bhowmik, S. Bodoardo, I.E. Castelli, I. Cekic-Laskovic, R. Christensen, S. Clark, R. Diehm, R. Dominko, M. Fichtner, A. A. Franco, A. Grimaud, N. Guillet, M. Hahlil, S. Hartmann, V. Heiries, K. Hermansson, A. Heuer, S. Jana, L. Jabbour, J. Kallo, A. Latz, H. Lorrman, O. M. Løvvik, S. Lyonnard, M. Meeus, E. Paillard, S. Perraud, T. Placke, C. Punckt, O. Raccurt, J. Ruhland, E. Sheridan, H. Stein, J. M. Tarascon, V. Trapp, T. Vegge, M. Weil, W. Wenzel, M. Winter, A. Wolf, K. Edström, *Adv. Energy Mater.* **2022**, *12*, 2102785.
[5] S. Xu, J. Zhou, J. Wang, S. Pathiranage, N. Oncel, P. Robert llango, X. Zhang, M. Mann, X. Hou, *Adv. Funct. Mater.* **2021**, *31*, 2101645.
[6] J. Moon, H. C. Lee, H. Jung, S. Wakita, S. Cho, J. Yoon, J. Lee, A. Ueda, B. Choi, S. Lee, K. Ito, Y. Kubo, A. C. Lim, J. G. Seo, J. Yoo, S. Lee, Y. Ham, W. Baek, Y. G. Ryu, I. T. Han, *Nat. Commun.* **2021**, *12*, 2714.
[7] A. J. Louli, L. D. Ellis, J. R. Dahn, *Joule* **2019**, *3*, 745–761.
[8] A. J. Louli, J. Li, S. Trussler, C. R. Fell, J. R. Dahn, *J. Electrochem. Soc.* **2017**, *164*, A2689-A2696.
[9] A. Manthiram, B. Song, W. Li, *Energy Storage Mater.* **2017**, *6*, 125–139.
[10] M. Jiang, D. L. Danilov, R. A. Eichel, P. H. L. Notten, *Adv. Energy Mater.* **2021**, *11*, 2103005.
[11] H. Q. Pham, E. H. Hwang, Y. G. Kwon, S. W. Song, *Chem. Commun.* **2019**, *55*, 1256–1258.
[12] M. Chen, C. Ma, Z. Ding, L. Zhou, L. Chen, P. Gao, W. Wei, *ACS Energy Lett.* **2021**, *6*, 1280–1289.
[13] R. Gond, W. van Ekeren, R. Mogensen, A. J. Naylor, R. Younesi, *Mater. Horiz.* **2021**, *8*, 2913–2928.
[14] X. Fan, C. Wang, *Chem. Soc. Rev.* **2021**, *50*, 10486–10566.
[15] M. Li, C. Wang, Z. Chen, K. Xu, J. Lu, *Chem. Rev.* **2020**, *120*, 6783–6819.
[16] T. Li, X.-Q. Zhang, P. Shi, Q. Zhang, *Joule* **2019**, *3*, 2647–2661.
[17] O. Borodin, J. Self, K. A. Persson, C. Wang, K. Xu, *Joule* **2020**, *4*, 69–100.
[18] X. Fan, L. Chen, X. Ji, T. Deng, S. Hou, J. Chen, J. Zheng, F. Wang, J. Jiang, K. Xu, C. Wang, *Chem* **2018**, *4*, 174–185.
[19] X. Ren, L. Zou, X. Cao, M. H. Engelhard, W. Liu, S. D. Burton, H. Lee, C. Niu, B. E. Matthews, Z. Zhu, C. Wang, B. W. Arey, J. Xiao, J. Liu, J.-G. Zhang, W. Xu, *Joule* **2019**, *3*, 1662–1676.
[20] S. Chen, J. Zheng, D. Mei, K. S. Han, M. H. Engelhard, W. Zhao, W. Xu, J. Liu, J.-G. Zhang, *Adv. Mater.* **2018**, *30*, 1706102.
- [21] D. J. Yoo, S. Yang, K. J. Kim, J. W. Choi, *Angew. Chem. Int. Ed.* **2020**, *59*, 14869–14876; *Angew. Chem.* **2020**, *132*, 14979–14986.
[22] S. Ji, J. Li, J. Li, C. Song, S. Wang, K. Wang, K. S. Hui, C. Zha, Y. Zheng, D. A. Dinh, S. Chen, J. Zhang, W. Mai, Z. Tang, Z. Shao, K. N. Hui, *Adv. Funct. Mater.* **2022**, *32*, 2200771.
[23] K. Xu, S. Zhang, J. L. Allen, T. R. Jow, *J. Electrochem. Soc.* **2003**, *150*, A170–A175.
[24] M. Zhou, C. Qin, Z. Liu, L. Feng, X. Su, Y. Chen, L. Xia, Y. Xia, Z. Liu, *Appl. Surf. Sci.* **2017**, *403*, 260–266.
[25] H. F. Xiang, H. W. Lin, B. Yin, C. P. Zhang, X. W. Ge, C. H. Chen, *J. Power Sources* **2010**, *195*, 335–340.
[26] H. F. Xiang, H. Y. Xu, Z. Z. Wang, C. H. Chen, *J. Power Sources* **2007**, *173*, 562–564.
[27] L. Jiang, Q. Wang, K. Li, P. Ping, L. Jiang, J. Sun, *Sustainable Energy Fuels* **2018**, *2*, 1323–1331.
[28] L. Xia, Y. Xia, Z. Liu, *J. Power Sources* **2015**, *278*, 190–196.
[29] T. Dagger, P. Niehoff, C. Lünenbaum, F. M. Schappacher, M. Winter, *Energy Technol.* **2018**, *6*, 2023–2035.
[30] J. Liu, X. Song, L. Zhou, S. Wang, W. Song, W. Liu, H. Long, L. Zhou, H. Wu, C. Feng, Z. Guo, *Nano Energy* **2018**, *46*, 404–414.
[31] K. Xu, M. S. Ding, S. Zhang, J. L. Allen, T. R. Jow, *J. Electrochem. Soc.* **2002**, *149*, A622–A626.
[32] D. H. Jeon, *Energy Storage Mater.* **2019**, *18*, 139–147.
[33] A. Davoodabadi, C. Jin, D. L. Wood III, T. J. Singler, J. Li, *Extreme Mech. Lett.* **2020**, *40*, 100960.
[34] E. Peled, S. Menkin, *J. Electrochem. Soc.* **2017**, *164*, A1703–A1719.
[35] Q. Liu, Z. Chen, Y. Liu, Y. Hong, W. Wang, J. Wang, B. Zhao, Y. Xu, J. Wang, X. Fan, L. Li, H. B. Wu, *Energy Storage Mater.* **2021**, *37*, 521–529.
[36] M. Gleria, R. Bertani, R. De Jaeger, S. Lora, *J. Fluorine Chem.* **2004**, *125*, 329–337.
[37] W. Choi, H.-C. Shin, J. M. Kim, J.-Y. Choi, W.-S. Yoon, *J. Electrochem. Sci. Technol.* **2020**, *11*, 1–13.
[38] S. K. Heiskanen, J. Kim, B. L. Lucht, *Joule* **2019**, *3*, 2322–2333.
[39] Y. Lin, J. Jiang, Y. Zhang, X. He, J. Ren, P. He, C. Pang, C. Xiao, D. Yang, N. Du, *Chem. Mater.* **2020**, *32*, 6365–6373.
[40] S. Jiang, B. Hu, R. Sahore, L. Zhang, H. Liu, L. Zhang, W. Lu, B. Zhao, Z. Zhang, *ACS Appl. Mater. Interfaces* **2018**, *10*, 44924–44931.
[41] C. Li, T. Shi, D. Li, H. Yoshitake, H. Wang, *RSC Adv.* **2016**, *6*, 34715–34723.
[42] W. Wang, H. Hu, X. Zeng, W. Fan, T. Yang, X. Zhao, C. Fan, X. Zuo, J. Nan, *ACS Appl. Mater. Interfaces* **2021**, *4*, 7101–7111.
[43] J. Feng, Y. An, L. Ci, S. Xiong, *J. Mater. Chem. A* **2015**, *3*, 14539–14544.
[44] V. Nilsson, S. Liu, C. Battaglia, R.-S. Künnel, *Electrochim. Acta* **2022**, *427*, 140867.
[45] W. Zhao, L. Zou, H. Jia, J. Zheng, D. Wang, J. Song, C. Hong, R. Liu, W. Xu, Y. Yang, J. Xiao, C. Wang, J.-G. Zhang, *ACS Appl. Mater. Interfaces* **2020**, *3*, 3369–3377.
[46] A. V. Marenich, C. J. Cramer, D. G. Truhlar, *J. Phys. Chem. B* **2009**, *113*, 6378–6396.
[47] A. Ghaur, C. Peschel, I. Dienwiebel, L. Haneke, L. Du, L. Profanter, A. Gomez-Martin, M. Winter, S. Nowak, T. Placke, *Adv. Energy Mater.* **2023**, 2203503. <https://doi.org/10.1002/aenm.202203503>.

Manuscript received: May 25, 2023

Revised manuscript received: May 31, 2023

Version of record online: June 18, 2023